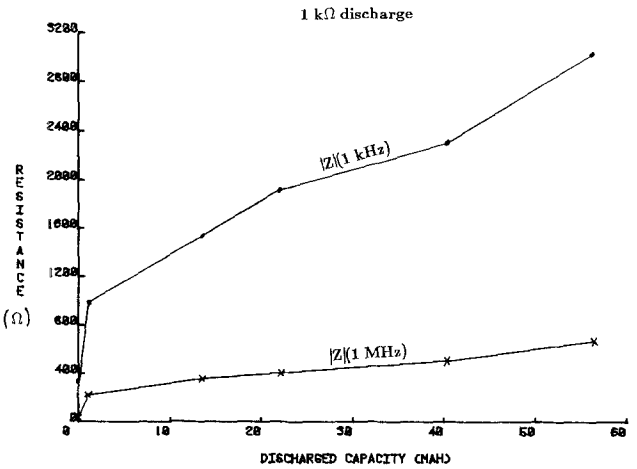

Fig. 6. |Z|(1 kHz), |Z|(1 MHz) *vs.* discharged capacity for 1 kΩ discharge.

impedance at 1 kHz, |Z|(1 kHz), which includes both the cathode and LiI impedances, and that at 1 MHz, |Z| (1 MHz), which is approaching the cathode impedance alone, as a function of discharged capacity. Obviously, even at this high discharge rate, the cathode impedance is small with respect to the electrolyte impedance. The 1 MHz impedance is actually an overestimate of the cathode impedance due to a partial contribution of the capacitive portion of the LiI electrolyte impedance. While it would have been preferable to have followed the actual cathode impedance as a function of depth of discharge, the assumption used in recent work (2) that the cathode impedance of these cells is small with respect to the LiI impedance has been confirmed.

An evaluation of the data showed that the 1 MHz value was approximately 20% of the 1 kHz value for cells discharged across either 20 or 1 kΩ, and remained so for most of the discharge. As expected, as the cell began to near the end of life, the cathode impedance rose dramatically.

Summary

A low cost, low power, high frequency galvanostat has been constructed and applied to discharging Li/I_2 batteries. The galvanostat, based upon a design for a voltage-controlled current source in a popular electronics text, has a bandwidth of 1 MHz throughout which it does not significantly distort the shape of the sinusoidal input. While 1 MHz is not sufficient in all cases for a complete impedance spectrum to be generated, this work does provide an economical extension of present capabilities.

After this initial development work, a number of ways in which the performance of the galvanostat can be improved are obvious. Replacement of the operational amplifiers with transistor amplifiers will increase the speed of the system. A number of design changes aimed at reducing the capacitive effects in the transistors will also serve to increase the speed of the instrument. Other design changes should allow an improved utilization of the large gain-bandwidth products of commercial transistors. A typical value for the transistors used in the present design is 1800 MHz. This would allow the transistors to have a gain of 180 at 10 MHz. This should allow development of a galvanostat able to operate at 10 MHz. Institution of wide bandwidth amplifiers for the output signals would give the transient analyzer more signal with which to work. In summary, both design and component changes should be able to improve the performance of the instrument to enable measurements to be made at 10 MHz. At such frequencies, other problems begin to loom ever larger, such as impedance matching of measuring devices. However, through careful design, such problems should be manageable.

In addition to developing a high speed galvanostat for general use, another goal of this summer project was to analyze the validity of an assumption made in previous work on Li/I_2 batteries (2, 3). In that work, it was assumed that the bulk of the increases in the impedance measured at approximately 1 kHz was due to increases in the LiI electrolyte resistance. However, due to the limited conductivity of the cathodes in these cells, there was a concern about the validity of this assumption at high discharge rates, and an interest in the way in which the cathode impedance changed as a function of discharge rate and depth. Though it was found that 1 MHz is not a sufficiently high frequency to completely separate the LiI and cathode impedances, it was high enough to show that the cathode impedance is, at most, 20% of the LiI impedance over the range of capacities of interest.

Acknowledgments

The author would like to thank The Electrochemical Society and the Department of Energy for the opportunity to do this work through an Energy Research Summer Fellowship. The generous support of the Catalyst Research Corporation is also gratefully acknowledged. The assistance of Professors James Wagner and Louis Phillips in the choice of components for and analysis of the circuit was instrumental. Professors Eliezer Gileadi and Patrick Moran were sources of constant encouragement and helpful discussions throughout this entire project.

REFERENCES

1. C. F. Holmes, in "Batteries for Implantable Biomedical Devices," B. B. Owens, Editor, p. 175, Plenum Press, New York (1986).
2. R. G. Kelly, M.S.E. Thesis, The Johns Hopkins University, Baltimore, MD (1986).
3. R. G. Kelly and P. J. Moran, *This Journal*, **134**, 25 (1987).
4. R. G. Kelly, P. J. Moran, *ibid.*, **134**, 31 (1987).
5. D. Surd, J. Jolson, N-L. Yang, and C. J. Hou, Presented at the 1985 Power Sources Conference, Cherry Hill, NJ, 1985.
6. P. Horowitz and W. Hill, "The Art of Electronics," p. 97, Cambridge University Press, New York (1980).
7. A. Vladimirescu, K. Zhang, A. R. Newton, D. O. Pederson, and A. Sangiovanni-Vincentelli, "SPICE Version 2G User's Guide," University of California, Berkeley, CA (1981).

Juhyoun Kwak is a graduate student in Chemistry at the University of Texas at Austin. He received a B.S. degree in Chemistry in 1978 and a M.S. degree in Analytical Chemistry in 1980 from Seoul National University in Korea. He is currently working toward his Ph.D. on the theory and application of ultramicroelectrodes in highly resistive media.

Mr. Kwak's report is given below.

Digital Simulation of Linear Sweep Voltammetry of Quasi-Reversible Systems at Ultramicroelectrodes

Ultramicroelectrodes are advantageous in highly resistive media (1, 2) or at fast scan rates in cyclic voltammetry experiments (3, 4) because of the small IR drop compared to that of conventional sized electrodes. Another advantage arises from nonlinear diffusion at ultramicroelectrodes, which results in higher mass-transfer rates. A general review of ultramicroelectrodes in electrochemistry has appeared (5). This review also mentions the application of ultramicroelectrodes as sensors, *e.g.*, to allow the monitoring of chemical changes *in vivo*. Electrochemistry at ultramicroelectrodes in highly resistive media has been of special interest (1, 2, 6). In dealing with these media, especially when direct electrolysis of the solvent is considered (7), the effect of elec-

tric fields on the migration of reactants and products must be considered in obtaining the theoretical current-potential behavior. We are developing a digital simulation algorithm for the migration-diffusion process at spherical electrodes. As a first stage, the algorithm has been checked with simpler electrochemical systems. Typical results for linear sweep and cyclic voltammetry of quasi-reversible systems at spherical electrodes in the absence of migration effects will be presented. The theoretical treatment of this case has not been presented previously. For example, Nicholson and Shain (8, 9) do not provide the spherical correction for quasi-reversible systems as they did for other systems. We note that the spherical electrode geometry (one-dimensional space problem) is a good approximation to the microdisk electrode geometry (two-dimensional space problem) as discussed later.

A number of methods (10-12) to solve the continuum mechanics diffusion process model represented by partial differential equations are available. For simplicity, the explicit finite-difference method was selected to simulate the diffusion process at spherical electrodes. A general procedure for this method has been described by Feldberg (10). In this method, space and time can be divided into arbitrary or nonuniform grids (13). In this work, the algorithm based on an exponentially expanding space grid for spherical geometry and a linear time grid (14) was used for rapid computation. In the application of this simulation to ultramicroelectrode theory, one more parameter, which depends on the size of the electrode, must be added to the parameters for a planar electrode (8, 15).

Simulated Results and Discussion

As shown by Fleishmann *et al.* (15), the steady-state diffusion limited current density at a microdisk electrode of radius a, can be approximated by that at a spherical electrode of radius $r_0 = (\pi/4)a$. The maximum currents at both electrodes converge to that at the planar electrode at fast scan rates in linear sweep voltammetry, when nonlinear contributions to diffusion become negligible. To satisfy the above two conditions and to approximate a microdisk electrode by a spherical one, a spherical surface subtending a solid angle of 1.6 π embedded in an insulating matrix was used. This electrode geometry is close to that of a hemispherical electrode with a solid angle of 2π. The maximum current, I_m, for the reversible

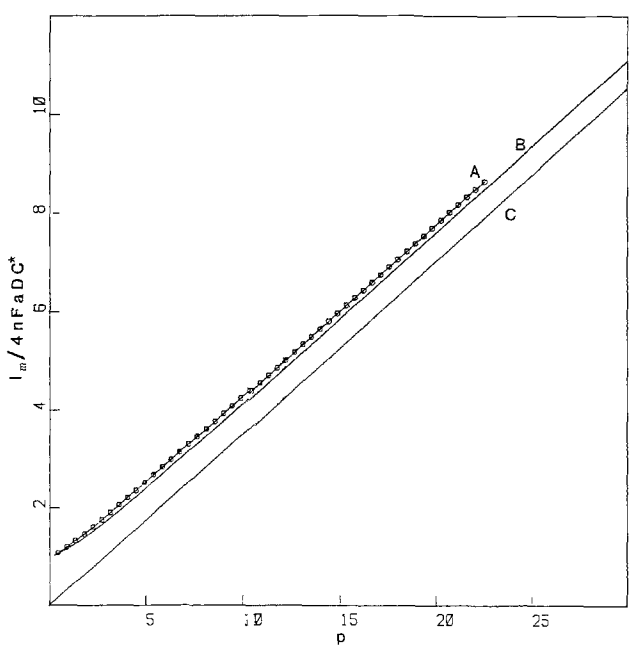

Fig. 1. $I_m/4nFADC^*$ as a function of $p = (nFa^2v/RTD)^{1/2}$ in linear sweep voltammetry on reversible systems at three different electrodes: (A) 1.6 π solid-angle spherical electrodes; (B) microdisk electrodes; and (C) planar electrodes.

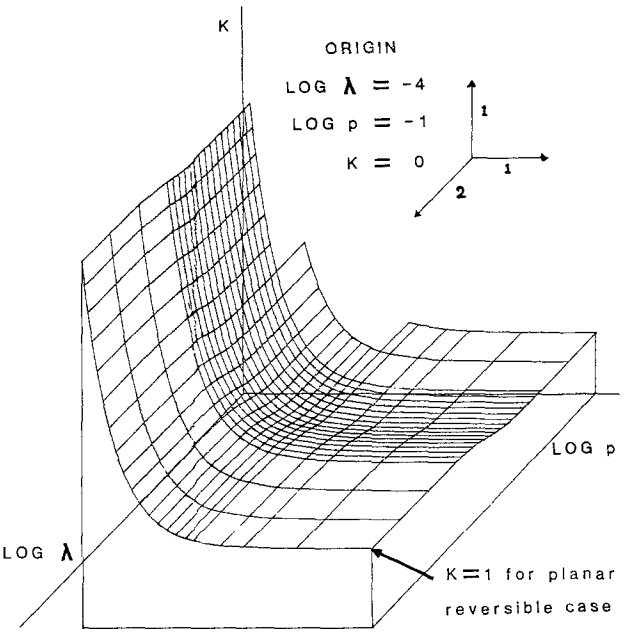

Fig. 2. Linear sweep voltammetric response at 1.6 π solid-angle spherical electrodes for $\alpha = 0.5$ and $D = D_A = D_B$. $K = I_m/I_{p,}$ planar, rev as a function of $p = (nFa^2v/RTD)^{1/2}$ and $\lambda = k^\circ/[D(nF/RT)v]^{1/2}$. $I_{p,}$ planar, rev is the reversible peak current at planar electrode.

case at a spherical electrode is compared with that of the microdisk electrode from the functional form of Aoki *et al.* (17). In Fig. 1, the maximum currents, I_m, for the above two electrodes as a function of dimensionless parameter $p = (nFa^2v/RTD)^{1/2}$ are shown, including that of planar electrode. From this figure, it can be said that the linear sweep voltammetric characteristics of a microdisk electrode are between those of a planar electrode and those of a 1.6 π solid angle spherical electrode, and closer to the latter. In other words, the characteristics of a microdisk electrode more quickly converge to those of a planar electrode than those of a 1.6 π solid angle spherical electrode when the scan rate is increased. Qualitatively, the above result might be explained as follows: the curvature effect at spherical electrodes comes from the entire electrode surface, but the edge effect at microdisk electrodes comes only from the edge. The relative error of the maximum current between the two geometries is less than 5%, so the spherical electrode is a good approximation to the microdisk and its use reduces the number of spatial dimension parameters that must be employed in the simulations.

Although linear sweep voltammetry of quasi-reversible systems has been simulated at microdisk electrodes by Heinze (18), a data treatment, similar to that at a planar electrode by Matsuda and Ayabe (20), was not presented. To consider both the nonlinear diffusion at ultramicroelectrodes and the variation in heterogeneous electron-transfer kinetics, it is useful to use two dimensionless parameters, p and λ, where $p = (nFa^2v/RTD)^{1/2}$, as used by Aoki *et al.* (17), and $\lambda = k^\circ/[D(nF/RT)v]^{1/2}$, as used by Matsuda and Ayabe (20). In the full domain of two dimensionless parameters, the maximum current was obtained by digital simulation. Typical results for the maximum current for $\alpha = 0.5$ are shown in Fig. 2. As expected, the results converge to those of Matsuda and Ayabe as $p \to \infty$ and of Aoki *et al.* as $\lambda \to \infty$. The full variation of other variables (*i.e.*, α and $\xi = (D_0/D_R)^{1/2}$) can be simulated and analyzed in the same way and should show similar trends.

In conclusion, these results not only complete the theory of linear sweep voltammetry at spherical electrodes, but also provide a treatment of quasi-reversible heterogeneous kinetics at a microdisk electrode.

Acknowledgment

The author is grateful to The Electrochemical Society for its generous support through an Energy Research

Summer Fellowship. The careful direction and continuous support of A. J. Bard is appreciated. Also, the author would like to thank S. W. Feldberg at Brookhaven National Laboratory for the detailed discussion and help in the finite-difference method.

REFERENCES

1. A. M. Bond, M. Fleischmann, and J. Robinson, *J. Electroanal. Chem.*, **168,** 299 (1984).
2. J. Cassidy, S. B. Khoo, S. Pons, and M. Fleischmann, *J. Phys. Chem.*, **89,** 3933 (1985).
3. J. O. Howell and R. M. Wightman, *Anal. Chem.*, **56,** 524 (1984).
4. J. O. Howell, J. M. Goncalves, C. Amantore, L. Klasinc, R. M. Wightman, and J. K. Kochi, *J. Am. Chem. Soc.*, **106,** 3968 (1984).
5. R. M. Wightman, *Anal. Chem.*, **53,** 1125A (1981).
6. A. M. Bond, M. Fleischmann, and J. Robinson, *J. Electroanal. Chem.*, **172,** 11 (1984).
7. R. A. Malmsten and H. S. White, *This Journal*, **133,** 1067 (1986).
8. R. S. Nicholson, *Anal. Chem.*, **37,** 1351 (1965).
9. R. S. Nicholson and I. Shain, *ibid.*, **36,** 706 (1964).
10. S. W. Feldberg, in "Electroanalytical Chemistry," Vol. 3, A. J. Bard, Editor, Marcel Dekker, New York (1969).
11. B. S. Pons, in "Electroanalytical Chemistry," Vol. 13, A. J. Bard, Editor, Marcel Dekker, New York (1984).
12. O. S. Ksenzhek and G. A. Lobach, *Sov. Electrochem.*, **18,** 1352 (1982).
13. T. Joslin and D. Pletcher, *J. Electroanal. Chem.*, **49,** 171 (1974).
14. S. W. Feldberg, *ibid.*, **127,** 1 (1981).
15. H. Matsuda and Y. Ayabe, *Z. Elektrochem.*, **59,** 494 (1955).
16. M. Fleischmann, F. Lassere, J. Robinson, and D. Swan, *J. Electroanal. Chem.*, **177,** 115 (1984).
17. K. Aoki, K. Akimoto, K. Tokuda, H. Matsuda, and J. Osteryoung, *ibid.*, **171,** 219 (1984).
18. J. Heinze, *Ber. Bunsenges. Phys. Chem.*, **85,** 1096 (1981).

In-Hyeong Yeo was born in Dae Jon, Korea, where he received his elementary and secondary education. He attended Sogang University in Seoul, Korea, where he received his B.S. degree in 1978 and, in 1983, his M.S. degree in Physical Chemistry. Since July 1983, he has been a Ph.D. candidate at Iowa State University in Ames, Iowa, where he has worked under the supervision of Professor Dennis C. Johnson.

Mr. Yeo's report appears below.

Electrocatalytic Oxygen Transfer Reactions at PbO_2 and Modified PbO_2 Electrodes

Lead dioxide applied as an anode material for electroanalysis and electrosynthesis has the desirable qualities of high electronic conductivity and a large positive working range due to the large activation overpotential for the evolution of oxygen by decomposition of water. It also has been shown (1) that PbO_2 anodes have significantly greater electrocatalytic activity than other common anode materials (*i.e.*, Pt, Au, and C) for supporting anodic processes in which oxygen is transferred from H_2O to the oxidation product.

The high oxygen transfer electrocatalytic activity is concluded to be the result of the fact that PbO_2 is a nonstoichiometric oxide, indicating a defect structure that results, most probably, in some surface sites at which oxygen is not bound with a high surface lattice energy. However, there remain many reactions for which the anodic oxygen transfer rate is not sufficiently fast to allow for transport-controlled reaction rates. An example is the oxidation of Mn(II) to MnO_4^-.

Table I. Number of oxygen atoms per metal atom and the unit areas of crystal faces for the rutile structure

Crystal faces	Area[b]	Number of oxygen atoms per metal atom
(100), (010)[a]	ac	0.119
(001)	ab	0.082
(011), (101)	$(a^2+c^2)^{1/2}\cdot a$	0.101
(110)	$\sqrt{2}ac$	0.042
(111)	$(a^2+2c^2)^{1/2}\cdot a$	0.059

[a]In the rutile structure, the (100) and (010) faces have the same area.
[b]a, b, and c represent the unit cell dimensions.

This research was motivated by the goal of increasing the electrocatalytic reactivity of electrodeposited lead dioxide for anodic oxygen transfer reactions. The determination of electrocatalytic activity for PbO_2 electrodes, as a result of the presence of other metal oxides, and the establishment of a possible mechanism of oxygen transfer catalysis at these electrodes were the principal goals of this research.

Previous studies (2) had observed the effects of doping for electrodeposited PbO_2 with rather large levels of Group III and V metal oxides. It was observed that doping with Group V oxides (*e.g.*, As_2O_5 and Bi_2O_5) results in significant increases in rates for numerous oxygen transfer reactions, whereas Group III oxides (*e.g.*, Tl_2O_3) decreased the rates below the values observed for pure PbO_2. For a PbO_2·Bi_2O_5 mixed oxide electrode, the rate constant for oxidation of Mn(II) is increased by more than 100 times, as compared with pure electrodeposited PbO_2. Other dramatic examples of an electrocatalytic effect are the oxidation of phenols, citric acids, and 2-thiophene carboxylic acid, all of which are inactive on pure electrodeposited PbO_2 electrodes.

X-ray diffraction (XRD) studies of the electrodes indicate that the mixed oxide maintains the crystal structure of pure β-PbO_2, *i.e.*, slightly distorted rutile, and Bi simply substitutes for Pb in the metal sites. The intensity of the peak at 2θ representing the (020) face is increased with increasing levels of Bi_2O_5, whereas the intensity of peaks representing the other faces (*e.g.* 121) decreases compared to pure β-PbO_2. This means that the crystals of PbO_2 deposited in the presence of Bi have grown in a way such that the (020) face is preferentially oriented parallel to the electrode. surface.

The ratio of oxygen to metal atoms on each of the principal crystal faces for β-PbO_2 was calculated using the Oak Ridge thermal ellipsoid plot program (ORTEP) (3). The results are summarized in Table I for five faces. As

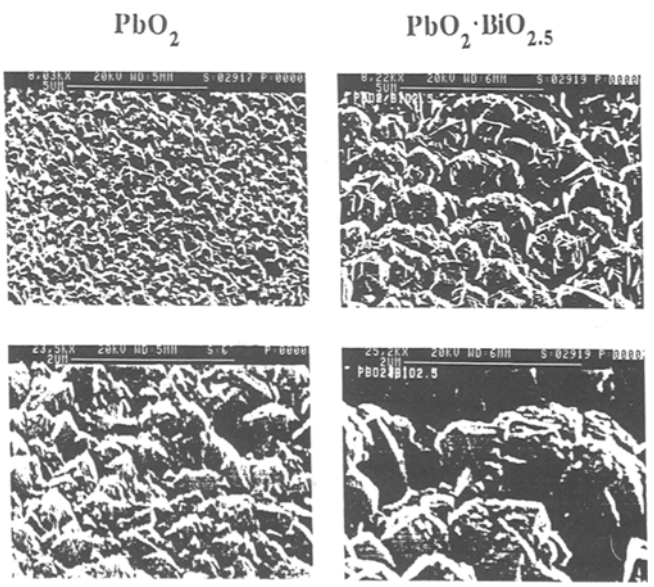

Fig. 1. Scanning electron micrographs of PbO_2 and PbO_2·$BiO_{2.5}$